Manuscript submitted February 10, 1997; revised manuscript received March 28, 1998.

Oki Electric Industry Company assisted in meeting the publication costs of this article.

REFERENCES

1. Y. Nishimoto, N. Tokumasu, T. Fukuyama, and K. Maeda, Ext. Abs. Conf. on Solid-State Dev. and Ma., p. 447 (1987).
2. H. Kotani, M. Matsuura, A. Fujii, H. Genjou, and S. Nagao, *Tech. Dig. Electron Devices Meet.*, 669 (1989).
3. K. Shimokawa, T. Usami, and M. Yoshimaru, *IEICE Trans.*, E77-C, 473 (1994).
4. M. Yoshimaru, T. Yoshie, M. Kageyama, K. Shimokawa, Y. Fukuda, and M. Ino, in *Proceedings of the IEEE International Reliability and Physics Conference*, p. 359, IEEE (1995).
5. K. Fujino, Y. Nishimoto, N. Tokumasu, and K. Maeda, *J. Electrochem. Soc.*, **137**, 2883 (1990).
6. K. Fujino, Y. Nishimoto, N. Tokumasu, and K. Maeda, *J. Electrochem. Soc.*, **138**, 550 (1991).
7. K. Kwok, E. Yieh, S. Robles, and B. C. Nguyen, *J. Electrochem. Soc.*, **141**, 2172 (1994).
8. K. Fujino, Y. Nishimoto, N. Tokumasu, and K. Maeda, *J. Electrochem. Soc.*, **139**, 1690 (1992).
9. N. Sato, T. Nakano, H. Yamamoto, and T. Ohta, *Jpn. J. Appl. Phys.*, **32**, L110 (1993).
10. M. Yoshimaru, N. Inoue, H. Tamura, and M. Ino, *IEEE Trans. Electron Devices*, **ED-41**, 1747 (1994).
11. L. L. Tedder, G. Lu, and J. E. Crowell, *J. Appl. Phys.*, **69**, 7037 (1991).
12. S. M. Hu, *J. Appl. Phys.*, **51**, 5945 (1980).
13. S. Fujimura, H. Ogawa, K. Ishikawa, C. Inomata, and H. Mori, Ext. Abs. 1993 Internat. Conf. on Solid-State Dev. and Mat., p. 618 (1993).
14. I. Tsuchiya, *J. Phys. Chem.*, **86**, 4107 (1982).
15. M. Kitagawa, H. Nishikawa, and Y. Ohki, *J. Appl. Phys.*, **74**, 2378 (1993).
16. T. Okuhara and J. M. White, *Appl. Surf. Sci.*, **29**, 223 (1987).
17. T. Satake, T. Sorita, H. Fujioka, H. Adachi, and H. Nakajima, *Jpn. J. Appl. Phys.*, **33**, 3340 (1994).
18. T. Sorita, S. Shiga, K. Ikuta, Y. Egashira, and H. Komiyama, *J. Electrochem. Soc.*, **140**, 2952 (1993).

Conduction Mechanism and Temperature-Dependent Current-Voltage in (Ba, Sr)TiO_3 Thin Films

M. S. Tsai and T. Y. Tseng

Department of Electronics Engineering and Institute of Electronics, National Chiao Tung University, Hsinchu 30050, Taiwan

ABSTRACT

RF magnetron sputtered (Ba, Sr)TiO_3 (BST) thin films were deposited on Pt/SiO substrate with various $O_2/(O_2 + Ar)$ mixing ratios (OMR) ranging from 0 to 60%. Two possible conduction mechanisms of the BST thin films, the Poole-Frenkel (PF) transport (bulk limited conduction) and the Schottky emission (SE) (electrode limited conduction) were studied. Experimental results indicated that the BST films prepared at low OMR (0-25%) exhibit the SE mechanism dominated below the transition electric field of 490 kV/cm and the PF transport mechanism dominated beyond 490 kV/cm; and while those prepared at high OMR (40-60%) display the SE mechanism dominated both below and beyond the transition electric field. The difference in dominant mechanism (bulk and electrode limited conduction) between films was ascribed to concentration variation of the oxygen vacancy in the films.

Introduction

The advancement of dynamic random access memories (DRAMs) has significantly decreased the available area per cell. (Ba, Sr)TiO_3 (BST) thin films with a high dielectric constant have attracted great attention for practical use in a capacitor of gigabit era DRAMs since the adoption of high-dielectric-constant materials can lower the height of the storage node and simplify the cell structure.[1-5] When they are incorporated into integrated circuits (ICs), leakage current in these capacitors is one of the most important parameters for estimating the capacitor charge retention. Therefore, the understanding of carrier transport in BST films has become important both from the fundamental and practical points of view. Although several conduction mechanisms have been reported to describe the conduction of the ferroelectric thin film capacitors, some controversies still exist regarding the major electrical leakage mechanisms as suggested by different authors depending on the system used, i.e., the dielectric and electrode materials.[6-11] It is known that oxygen vacancies in BST films play a prominent role in leakage current of the films.[12] No mention was made of the correlation between concentration of the oxygen vacancies of the films and their leakage current conduction mechanisms. We have reported on the electrical and physical properties of BST thin films on Pt/SiO_2/Si substrates prepared by radio frequency (rf) magnetron sputtering at various $O_2/(O_2 + Ar)$ mixing ratios (OMR).[13] This work has been attempted to clarify the correlation between electrical leakage mechanisms and possible concentration variation of oxygen vacancies in the films deposited at various OMR. For this purpose, BST films have been deposited at various OMR. Electrical performance of these films is examined and their possible conduction mechanisms will be discussed.

Experimental

BST thin films were deposited on Pt/SiO_2/p-Si(100) bottom storage node electrode by rf magnetron sputtering. Details of the preparation of BST thin films were described before.[13] The BST 50/50 targets with a 3 in. diam and a thickness of 0.25 in. were synthesized using a standard solid-state reaction process. All films were prepared at a fixed power of 100 W (power density is 2.26 W/cm^2) and a constant pressure of 10 mTorr which was maintained by a mixture of argon and oxygen at various mixing ratios ranging from 1:1.5 to 1:0. The target to substrate separation was about 5 cm. All the BST films was deposited at 450°C and has the same thickness of around 100 nm. The chemical composition of the films was close to the target composition within a deviation of 3% on the basis of measured results of the inductively coupled plasma atomic emission spectrometry (ICP-AES, Perking Elmer SCIEX ELAN 5000, U.S.) method. The 50 nm thick top Pt electrodes with diameters of 165, 255, and 350 μm were then formed by dual E-Gun deposition and patterned by the shadow mask process.

The film thickness was determined from ellipsometry. Secondary ion mass spectrometry (SIMS) measurement was performed in order to observe the variation of oxygen concentration in various OMR films. The capacitance-voltage

(C-V) characteristic was measured on the metal-insulator-metal (MIM) structure by measuring the capacitance at 100 kHz as a function of a swept positive-to-negative voltage bias. Dielectric constants of the films were calculated from capacitance measured at 100 kHz without bias voltage. The current-voltage (*I-V*) measurement was performed by measuring the current through the sample using HP4145B. A Pt top electrode of BST capacitor was connected to the voltage source, and the Pt bottom electrode was grounded. The polarity is positive when a positive voltage is applied to the top electrode. The direct current (dc) bias took the form of stepwise voltage ramps, then a leakage current was measured at each step. The height of each step (ΔV) is 0.01 V, a delay time (t_d) is 30 s and the retained time (t_m) after the delay time including the measurement time is 0.6 s. Thus the time interval of each step is 30.6 s. The current-time (*I-T*) measurement was performed by measuring the current through the samples using HP4145B. The measurement of leakage current was carried out at the period of dc application time with bias voltage.

Results and Discussion

The dependence of the dielectric constant and the leakage current density measured at 100 and 300 kV/cm with a delay time of 30 s on the OMR is shown in Fig. 1. The details were described in an earlier report.[13] The dielectric constant increased with increasing OMR, but it attained a maximum value at 50% OMR. Further increase of OMR decreased the dielectric constant. Leakage current density decreased with increasing OMR, but it had the minimum value of 40% OMR. The film deposited at 450°C and 50% OMR had a dielectric constant of 375 and leakage current density of 7.4×10^{-9} A/cm^2 at an electric field of 100 kV/cm with a delay time of 30 s. The leakage current of BST thin films greatly depends on the composition of the BST thin films, the bottom electrode materials, and grain size. The leakage current of our films was not significantly affected by the grain size, which was described in an earlier report.[13] The loss tangent of the films is also a function of OMR, as shown in Fig. 2. The film deposited at 450°C and 50% OMR has a loss tangent of 0.074 at 100 kHz. The minimum loss tangent occurs at OMR value of 40%, which is in good agreement with the leakage current results shown in Fig. 1.

Figure 3 indicates that the variation of leakage current with electric field (*J-E*) for the films prepared at various OMR. The leakage current has the minimum value at 40% OMR. If ohmic current dominates the leakage current at low electric field ($E < 100$ kV/cm), the slope, n, of log (J) vs. log (E) would be 1. The values n of 0, 25, 40, and 50% OMR are 0.12, 0.46, 0.43, and 0.38, respectively. Therefore, the *J-E* characteristics at low electric field in this experiment cannot be explained by ohmic current.

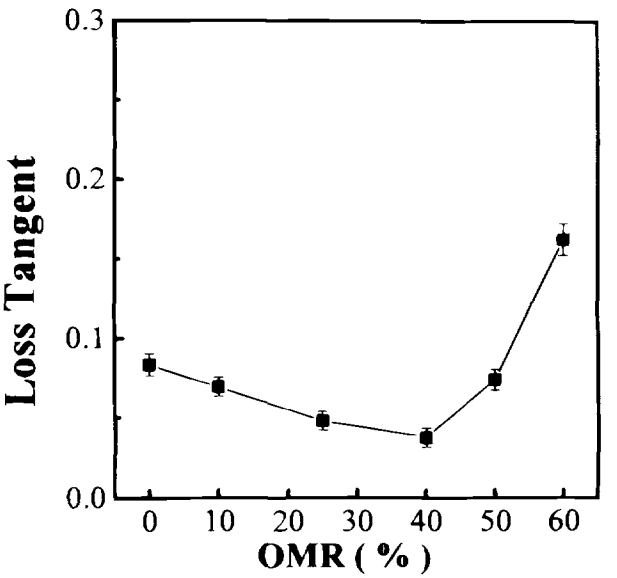

Fig. 2. The dependence of the loss tangent measured at 100 kHz on the OMR.

Figure 4 shows the leakage current density variation as a function of temperature of the films deposited at 0, 25, 40, 50, and 60% OMR, respectively, and measurements were carried out at 100 kV/cm. The leakage current increases with an increase in the measurement temperature, but this phenomenon may not be attributed to Fowler-Nordheim (FN) tunneling conduction mechanism which is inherently independent of the temperature. The Schottky emission (SE) mechanism and Poole-Frenkel (PF) transport which have been described in Ref. 12 may be employed to explain the temperature dependence.

Figure 5 shows the leakage current density variation as a function of the applied bias voltage of the films deposited at 0, 25, 40, and 50% OMR, respectively, and measurements were carried out at 27°C. In this work, we intend to verify that our Pt (top)/BST/Pt (bottom) capacitors have the PF transport (bulk limited conduction) at 0 and 25% OMR films, and an SE-type barrier (electrode limited conduc-

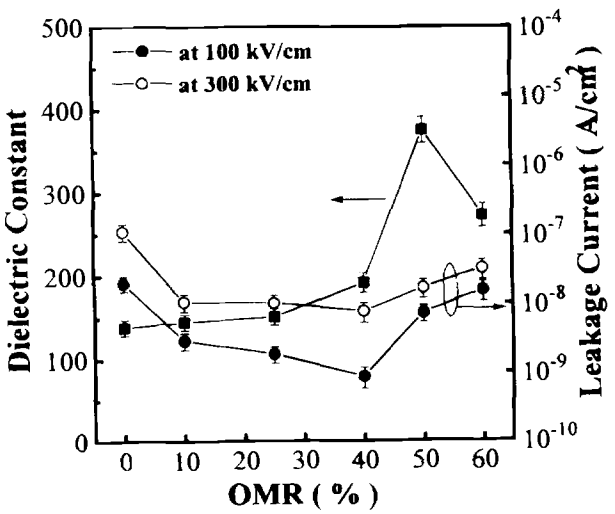

Fig. 1. The dependence of the dielectric constant and the leakage current density measured at 100 and 300 kV/cm with a delay time of 30 s on the OMR.

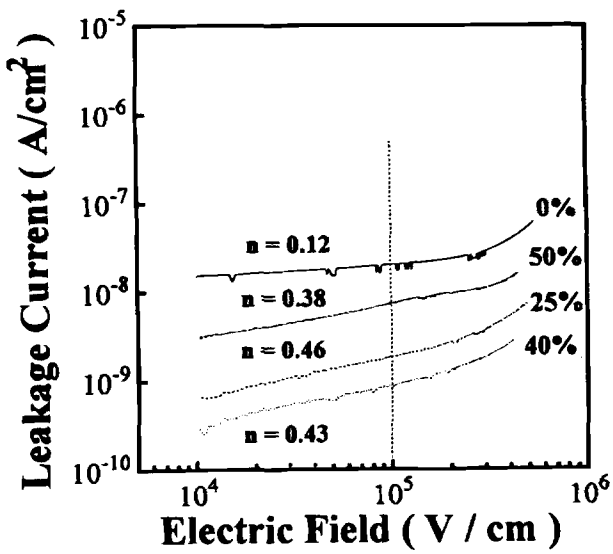

Fig. 3. The variation of leakage current with electric field for various OMR BST films.

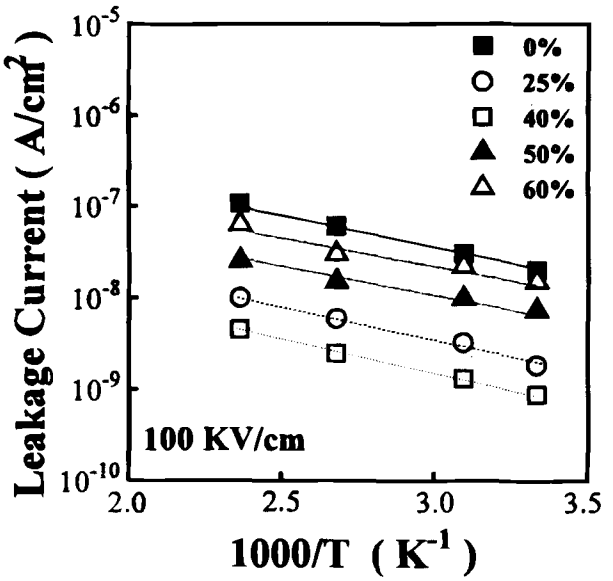

Fig. 4. Leakage current density vs. measurement-temperature for the BST thin film deposited at 0, 25, 40, 50, and 60% OMR.

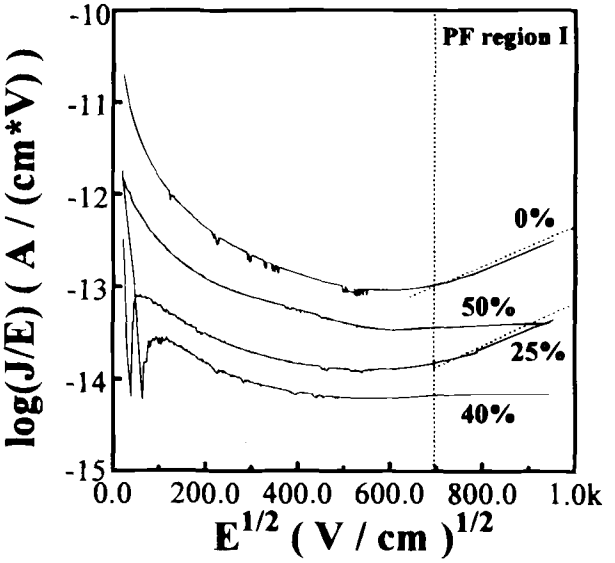

Fig. 6. The log (J/E) vs. $E^{1/2}$ plot showing the PF region for various OMR BST films.

tion) characteristic at 40 and 50% OMR films, based on the assumption that the BST thin film has an n-type conductivity. The n-type conductivity probably results from the oxygen vacancies or surface states such as surface adsorption and broken bonds.[10] SE is expected to occur at the interface between electrodes and dielectrics, where a Schottky barrier is formed. The Schottky barrier height is a function of the work function of the metal, electron affinity of the dielectric, and the surface states. If asymmetry of the metal-dielectric interface exists, leakage current will depend on applied voltage polarity, because the potential barrier which formed at the interface between top electrode and BST is not as high as that at the interface between bottom electrode and BST. PF transport involves a mechanism similar to SE, except that it is the lower barrier height of traps in the dielectric which excites electrons into the conduction band of the dielectric. Therefore, PF transport would not show polarity dependence, despite the existence of asymmetry of the electrode-dielectric interface. The most obvious candidate for a mobile defect that can be trapped at ferroelectric-electrode interfaces is the oxygen vacancy[14] which has been identified as being responsible for the degradation of the leakage current (dc degradation) in capacitors based on similar materials.[14]

The log(J/E) vs. $E^{1/2}$ curves for BST thin films deposited at 0, 25, 40, and 50% OMR shown in Fig. 6 indicate that the slopes for all the films below the transition electric field of 490 kV/cm have negative values, but the slopes for the 0 and 25% OMR films beyond the transition electric field change to positive values and show the linear relation. The similar behaviors appear in the log(J/T^2) vs. $E^{1/2}$ curves for the BST thin films deposited at 0, 25, 40, and 50% OMR, as shown in Fig. 7. For the 0 and 25% OMR BST films, the two step slopes were observed with the breaks at 490 kV/cm, and for the 40 and 50% OMR films, only the single slope can be observed. It is indicated that either the PF transport (Fig. 6) or the SE mechanism (Fig. 7) seems to be applicable to our samples.

Figure 5 also indicates that the leakage current density at negative bias (reverse current) is much higher than that at positive bias (forward current), the possible reasons may be: (*i*) the barrier height between BST film and bottom electrode interface is larger than that between BST film and top

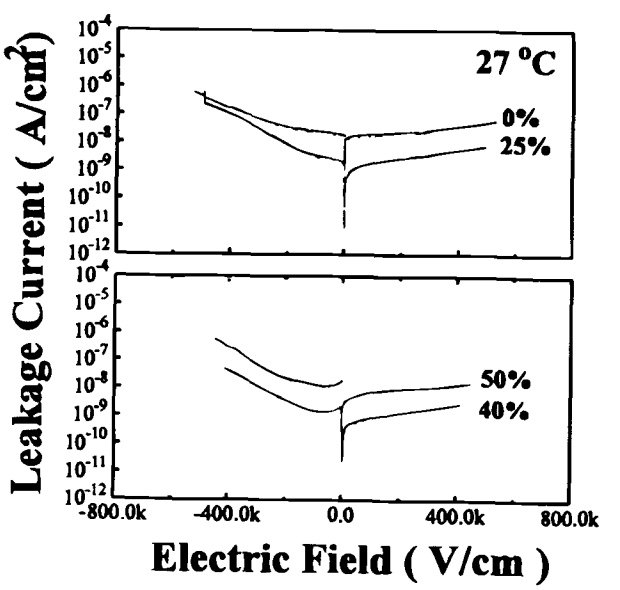

Fig. 5. Leakage current density vs. applied bias voltage for the BST thin film deposited at 0, 25, 40, and 50% OMR.

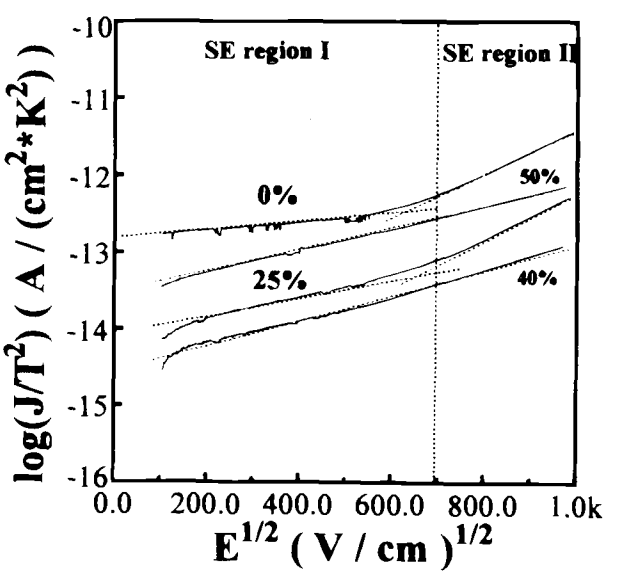

Fig. 7. The log (J/T^2) vs. $E^{1/2}$ plot showing the SE region for various OMR BST films.

electrode interface. Hwang et al.[9] attributed this potential barrier difference between two mentioned interfaces to the difference in the thermal history which the two interfaces experienced, and (*ii*) the root mean square (rms) surface roughness difference between the bottom electrode Pt and BST. Figure 8 shows the variation of rms surface roughness of the bottom electrode Pt and BST with various OMR. The BST film has a rougher surface than the bottom electrode Pt at various OMR. The surface roughness of BST films increases with increasing OMR. The details were described in an earlier report.[13] The above mentioned barrier height and surface roughness differences are such that the reverse current is much higher than the forward current. Joo et al.[15] assumed that the higher reverse current might be caused by a higher generation of oxygen vacancy in the BST film at the interface with the Pt top electrode. The deformation of the Pt electrode during the deposition of a lead zirconate titanate (PZT) ferroelectric thin film might cause stress creation in or distortion of the PZT film, consequently, the resulted defects or microcracks in the film might lead to increase the leakage current. Therefore, fabrication of a stable Pt electrode without deformation during the deposition of a PZT film and subsequent heat treatment was important for obtaining high-quality films with low leakage current.[16] The formation of possible hillocks on the bottom electrode Pt might also result in the large reverse current and appear current influence the asymmetry of *I-V* characteristics.[6]

The symmetric *J-E*, log (*J*/*E*) vs. $E^{1/2}$, and log (J/T^2) vs. $E^{1/2}$ curves for the BST thin films deposited at 27°C for 0 and 25% OMR are shown in Fig. 5, 6, and 7, which may suggest that the conduction mechanisms would be SE and PF at low (E < 490 kV/cm) and high (E > 490 kV/cm) electric fields, respectively. But at high measurement temperatures, the reversal of polarity of the applied field caused asymmetry in the *J-E* behavior (Fig. 9), indicating that the SE mechanism effect tends to increase. These phenomena may result from the higher oxygen vacancy-concentration existing in the films sputtered at 0 to 25% OMR. The high oxygen vacancies would lead to the increase in the trap centers. The accumulation of oxygen vacancies at the interface of top electrode Pt and BST occurs when negative bias is applied to the top electrode. The thermionic emission transport (SE mechanism) of electrons from the electrode over the interface-potential barrier into the BST thin film would be easy, because the barrier height is lowered by the image force and the surface trap state.[17,18] But the electrons over the interface-barrier are trapped by the trap centers due to

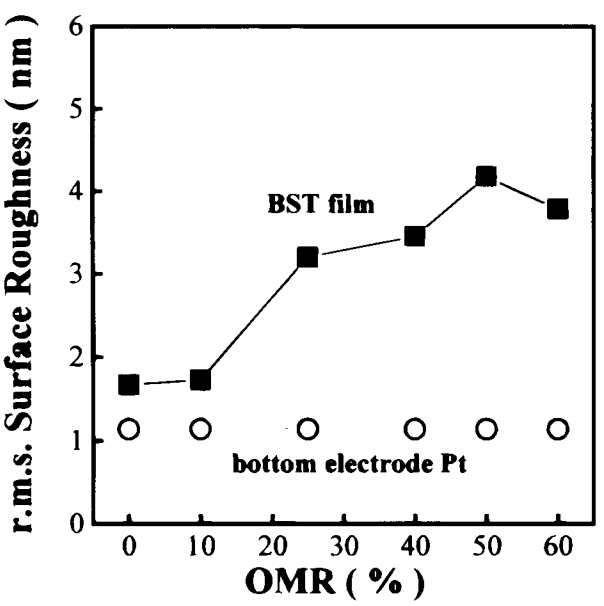

Fig. 8. The variations in rms surface roughness of the Pt bottom electrode and the BST film with various OMR.

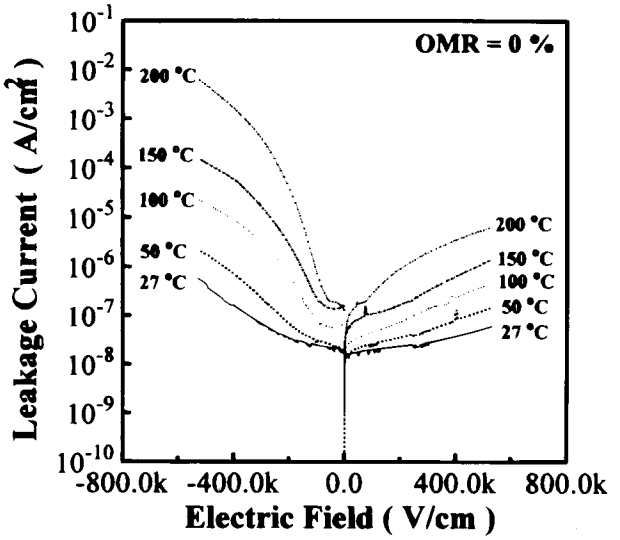

Fig. 9. Leakage current density vs. applied bias voltage for the BST thin film deposited at 0% OMR. The measurements were carried out at various temperatures.

the high oxygen vacancy concentration in the 0 and 25% OMR BST films. Therefore, the carriers that are thermally emitted from the trapped centers under a strong electric field (PF transport) dominate the leakage limited conduction mechanisms. Figure 9 shows the leakage current density variation as a function of the applied bias voltage of the film deposited at 0% OMR and measurements were carried out at 27, 50, 100, 150, and 200°C. At the high measurement temperature (T > 100°C), the electrons over the interface-barrier, with larger energy, can transport over the potential barrier of the trap centers and the possibility of electrons trapped by the oxygen vacancies will decrease, so the effect of SE limited mechanism will increase. Hence the *J-E* curve at high measurement temperature can be described as the combination of the SE emission and PF emission at high and low electric fields, but the SE emission dominates the electrical properties.

The reversal of polarity of the applied field caused asymmetry in the *J-E*, log (*J*/*E*) vs. $E^{1/2}$ and log (J/T^2) vs. $E^{1/2}$ curves of 40 and 50% OMR BST films as shown in Fig. 5, 6, and 7, indicating the formation of the SE mechanism-type barrier at the interface of the BST film and the Pt electrodes as mentioned later. The PF emission effect of *J-E* curve is eliminated because the oxygen vacancy defects decrease at higher OMR, so the main limiting conduction mechanism is the thermionic emission of electrons from the cathode electrode over the interface-barrier into the BST thin film. Therefore, the current-voltage characteristics are influenced by the SE conduction. The change of the film composition by OMR variation was analyzed using SIMS in detail to clarify the origin of conduction. Note that the oxygen concentration of BST films deposited at 0, 25, and 50% OMR increases with increasing OMR, as shown in Fig. 10a, b, and c. In fact, high temperature deposition of BST films under nonoxidizing atmosphere, such as Ar, generally produces oxygen vacancies in the film according to

$$O_O \rightleftarrows V_O^{\bullet\bullet} + 2e' + 1/2\ O_2 \qquad [1]$$

where O_O, $V_O^{\bullet\bullet}$, and e' represent the oxygen ion on its normal site, oxygen vacancy, and electron, respectively. As shown by Eq. 1, the BST material tends to show an n-type conductivity, although the conductivity is usually small due to the electrons produced with oxygen vacancies when the OMR is reduced.[13] Hence the possibility of the creation of oxygen vacancy defects may decrease at higher OMR. Leakage current density decreases with increasing OMR, but it has the minimum value of 40% OMR as shown in Fig. 1, because there is a change in dielectric loss.[13] In order to

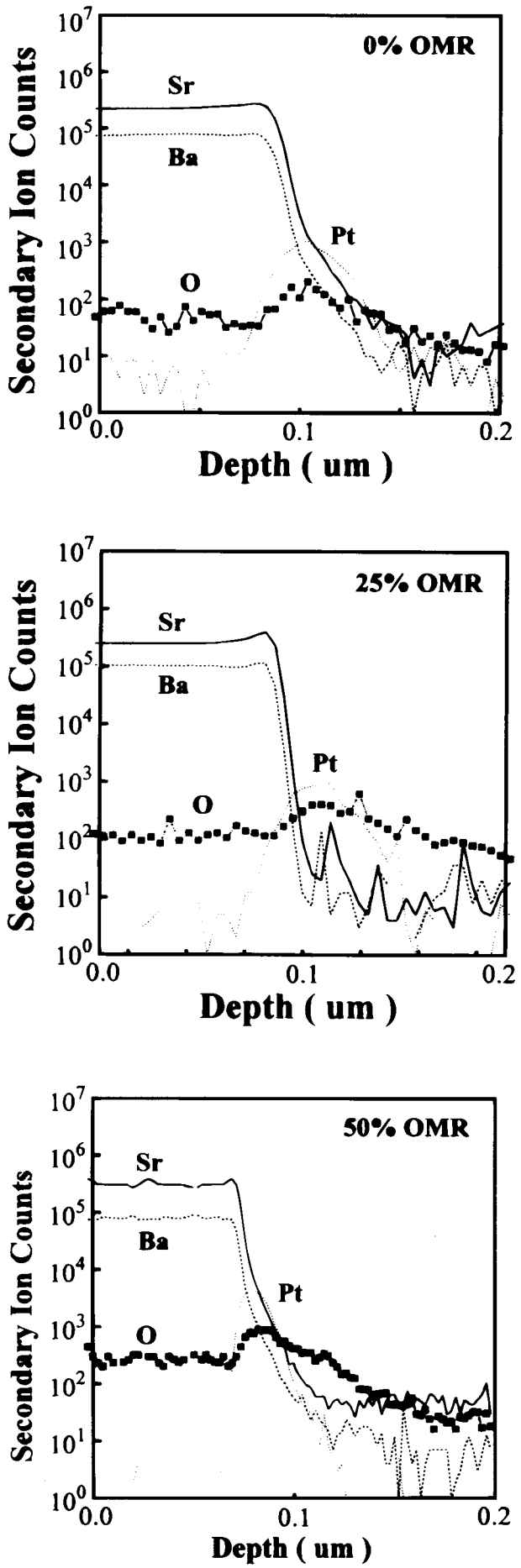

Fig. 10. The SIMS data of BST films deposited at (a, top) 0%, (b, middle) 25%, and (c, bottom) 50% OMR.

prove the existence of the variations in vacancy content, the study of the effect of oxidizing and reducing postdeposition heat-treatments on the leakage current density of BST films was carried out. The leakage current density of BST films after annealing in O_2 at 500 to 700°C for 1 to 30 min decreases. On the other hand, in comparison with the BST films without annealing, the BST films also annealed in forming gas (N_2/H_2 = 95/5) at 400°C for 30 min have lower dielectric constants and higher leakage currents, which may be attributed to the induced damage during hydrogen annealing process. That is, the active reduction and diffusion of hydrogen, even occurred at temperature as low as 350°C, may cause the activated hydrogen penetrated into BST and bottom electrode Pt, consequently, it may lead to chemical reaction and change in the BST/Pt interface. The damage may also take the form of oxygen vacancies which produce positively charged centers in BST films. The *J-E* behavior of 0 and 25% OMR BST as shown in Fig. 5, 6, and 7, indicating the formation of th SE mechanisms at low electric field (E < 490 kV/cm) and the PF mechanism at high electric field (E > 490 kV/cm). And the *J-E* behavior of BST at 40 and 50% OMR, indicating the formation of the SE mechanism at high and low electric fields.

The current transportation in BST films at high fields is normally attributed to either the SE or the PF mechanism. The leakage current J_{SE} governed by a SE mechanism is expressed as

$$J_{SE} = A^* T^2 \exp\{-q[\varphi_B - (qE/4\pi\epsilon_d\epsilon_o)^{1/2}]/kT\} \quad [2]$$

where A^* is a constant, φ_B is the potential barrier height on the surface, ϵ_d is the dynamic dielectric constant in ferroelectric material in the infrared region, q is the unit charge, k is Boltzmann's constant, T is temperature, and E is the external electric field.[17] The barrier height (φ_B) of SE mechanism is dependent on many parameters, such as the work function of the metal, electron affinity of semiconductor, barrier lowering by image force and the surface trap state.[17,18] The temperature and electric field dependences are mainly governed by φ_B and ϵ_d, respectively. The SE model can be modified to a PF-type conduction model if the conduction is governed by carriers that are thermally emitted from the trapped centers under a strong electric field.[19] The PF current, J_{PF}, is expressed as

$$J_{PF} = B\,E \exp\{-q[\varphi_t - (qE/\pi\epsilon_d\epsilon_o)^{1/2}]/kT\} \quad [3]$$

where B is a constant and φ_t a depth of trapped level.[17] Hence J_{SE} and J_{PF} are very similar; they are very hard to distinguish.

The slopes of linear region of the current-voltage (*J-E*) curves in the forms of ln (J/E) vs. $E^{1/2}$ and ln (J/T^2) vs. $E^{1/2}$ can be measured. The slope can also be calculated using the dielectric constant measured from an independent measurement. For the two different mechanisms, the slopes are obtained by the following relations

$$\beta_{SE} = q(q/4\pi\epsilon_d\epsilon_o)^{1/2}/kT \quad \text{for the SE mechanism} \quad [4]$$

$$\beta_{PF} = q(q/\pi\epsilon_d\epsilon_o)^{1/2}/kT \quad \text{for the PF mechanism} \quad [5]$$

The mechanism can be determined by comparing the slopes evaluated from an independent measurement of the dielectric constant with the slopes measured from *J-E* characteristics.[8] A related issue is choosing the value of ϵ_d, static or optical dielectric constant, to be used in describing the conduction mechanisms. Both the static and the optical dielectric constants are supported by the experimental data reported in the literature.[20-25] An effective dynamic dielectric constant has also been suggested to describe some experiments. The use of optical and static dielectric constants is dependent on how fast a carrier is assumed to move in the dielectric materials. The static dielectric constant should be used for a slow transport carrier and the optical constant for a fast transport carrier.

On the basis of Eq. 2 and 3, the activation energies, Ea^* listed in Table I, can be obtained from the slopes of the linear regions of the plots, log (J_{SE}/T^2) vs. T^{-1} (Fig. 11) and log

Table I. The activation energy (Ea^*) obtained from ln (J/T^2) vs. T^{-1} and ln (J/E) vs. T^{-1} plots of the 0, 25, 40, and 50% OMR BST capacitors at various fields as indicated.

		Activation Energy (Ea^*) (eV)				
	OMR (%)	50 kV/cm	75 kV/cm	100 kV/cm	125 kV/cm	150 kV/cm
ln (J/T^2) vs. T^{-1}	0	0.104	0.101	0.083	0.089	0.093
	25	0.116	0.116	0.081	0.074	0.068
	40	0.136	0.081	0.078	0.076	0.039
	50	0.092	0.045	0.039	0.039	0.039
ln (J/E) vs. T^{-1}	0	0.169	0.164	0.144	0.150	0.154
	25	0.180	0.180	0.178	0.135	0.129
	40	0.200	0.142	0.137	0.137	0.097
	50	0.156	0.106	0.100	0.100	0.099

(J_{PF}/E) vs. T^{-1} (Fig. 12), respectively, in the BST capacitors sputtered at 0, 25, 40, and 50% OMR at various fields indicated (positive bias was applied on the top electrode). Figures 11 and 12 are the typical plots for the BST capacitors deposited at 0% OMR. The activation energy increased with increasing OMR at 50 kV/cm, but it had the maximum value at 40% OMR. And the activation energy decreased with increasing electric field. An extrapolation of the activation energy (Ea^*) vs. the square root of the electric field curve gives φ_B for ln(J_{SE}/T^2) vs. T^{-1} and φ_t for ln(J_{PF}/E) vs. T^{-1}. The values of [φ_B(eV), φ_t(eV)] between 0, 25, 40, and 50% OMR films and bottom electrodes are (0.16, 0.23), (0.20, 0.27), (0.24, 0.31), and (0.14, 0.21), respectively, as shown in Fig. 13. The φ_B and φ_t increased with increasing OMR, but it had the maximum value at 40% OMR. A further increase of OMR decreased the potential-barrier height and the depth of trapped level. The results show that the barrier height is lowered by high concentration oxygen vacancies existed at lower OMR films, which leads to the depth of trap centers level φ_t near the surface (shallow trap level) (Fig. 13). Therefore, the electrons would be trapped easily, and the PF mechanism dominates the current transportation. For higher OMR film (40% OMR), the interface-barrier height and the depth of the trap center level are larger (deep trap level), so the SE mechanism dominates the electrical conduction. For 50% OMR film, the smaller values of interface-barrier height and the depth of the trap center level, and the larger leakage current may be attributed to that the polarization enhanced the electron-transport.[13] Additional mechanism such as relaxation loss may also be contributed to the increased conduction beyond 40% OMR. Therefore, the positive leakage current had the minimum value at 40% OMR, because there are the maximum values of activation energy, potential-barrier height, and trapped level (deep trap level) at 40% OMR. For the same reason, the negative leakage current density also had the minimum value at 40% OMR.

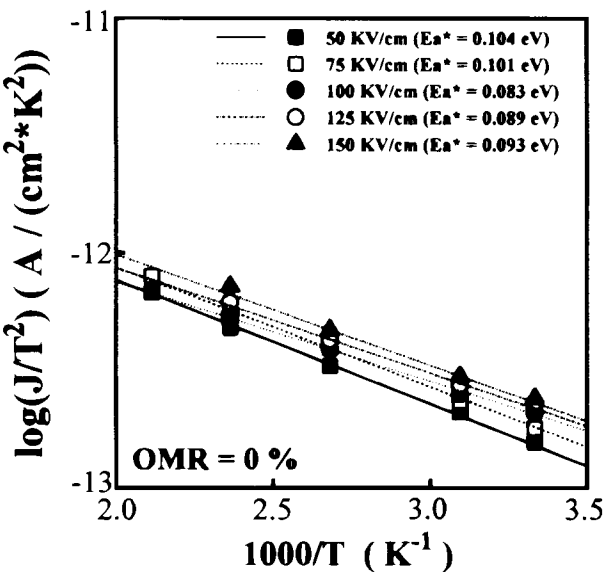

Fig. 11. log (J/T^2) vs. T^{-1} for the BST capacitors under various applied electric fields indicated.

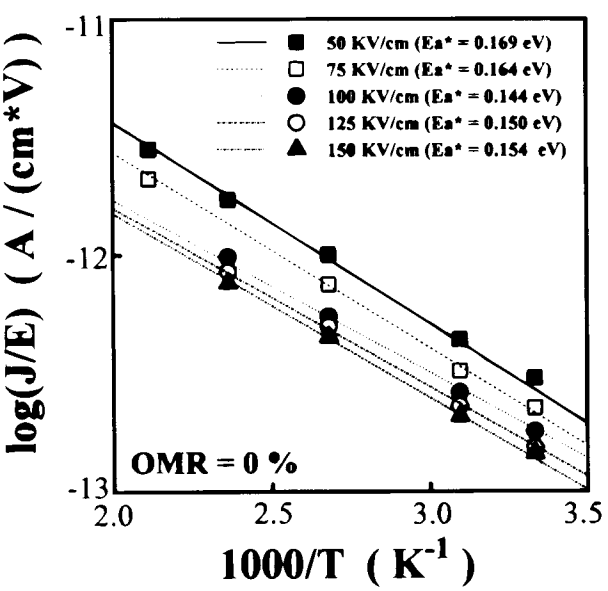

Fig. 12. log (J/E) vs. T^{-1} for the BST capacitors under various applied electric fields indicated.

As indicated in Fig. 6 and 7, either the PF transport (Fig. 6) or the SE mechanism (Fig. 7) can be applied to our samples. Table II lists the slopes of different linear regions of the plots shown in Fig. 6 and 7, the dynamic dielectric constant (ϵ_d) calculated on the basis of Eq. 2-5, the optical dielectric constant (ϵ_{op}) which is the square of the refractive index, and the static dielectric constant (ϵ_s) obtained from C-V measurement at 100 kHz.

It is indicated in Table II that the dynamic dielectric constants of 0% OMR films are 154 at SE region I and 113 at PF region I, which are in relatively close with the static dielectric constant, 138. Therefore, we suggest that the electronic carrier velocity is slow (polaron-like conduction) due to the existence of high concentration oxygen vacancies on 0% OMR films, so that the static dielectric constant would be used to describe the carrier transport through the films. The dynamic dielectric constants of 40 and 50% OMR films as shown in Table II are reduced, and the PF emission effect of the J-E curve is eliminated because the concentration of oxygen vacancy decreases at high OMR. The electron carrier velocity would be higher, so that the optical dielectric constant is expected to be used to describe the carrier transport through the films. The dominant conduction mechanism for high OMR films is the thermionic emission of electrons from the cathode electrode over potential-barrier into the thin film. Hence, the I-V characteristics are influenced by the SE mechanism.

Figure 14 shows the OMR dependence of current-time (J-t) characteristics of our BST thin films capacitors at 300 kV/cm. Possible causes for the time-dependent current are one or more of the following: (*i*) ionic drifting within the films, (*ii*) dipole polarization of the dielectric, and/or (*iii*) electronic charge trapping within the films. In general, if the electronic conduction is electrode limited and the time dependence is due to ionic drifting in solid, the magnitude of the electronic current increases with time, while both dipole polarization and charge trapping cause the current to decrease with time. Charge trapping results in field reduction at the injecting surface. As shown in Fig. 14, dipole polarization and/or charge trapping would be the dominant mechanism, giving the decrease in leakage current with time.

The J-t curves usually obey a power law, which is a linear dependence of log(J) vs. log(t), as indicated below

Table II. The calculated slopes of the various OMR BST films at room temperature by using various transport mechanisms, (positive bias was applied on the top electrode).

OMR (%)	SE (region I) β_{SE}	SE (region I) Dynamic dielectric constant	SE (region II) β_{SE}	SE (region II) Dynamic dielectric constant	PF (region I) β_{PF}	PF (region I) Dynamic dielectric constant	Static dielectric constant	Optical dielectric constant
0	1.18×10^{-3}	154	4.55×10^{-3}	10	2.76×10^{-3}	113	138	5.37
25	2.08×10^{-3}	50	3.72×10^{-3}	15	2.43×10^{-3}	145	151	5.43
40	2.53×10^{-3}	34	—	—	—	—	192	5.72
50	2.92×10^{-3}	25	—	—	—	—	375	5.48

$$J(t) = J_0 * t^{-n} \quad [6]$$

where n is an index of time dependence, and J_0 (A/cm^2) the current at $t = 1$ s. Table III lists the J_0 and n for various OMR films at various electric fields. The absorption current obeying Eq. 6 was known as having fractional power-law conductivity characteristics,[6] which can be explained by the models of distribution of relaxation times, one of which was a Maxwell model, which comprise an infinite number of resistor-capacitor series circuit in parallel. The combination with additional mechanism may be necessary for explaining an increase in the current and a decrease in n at high field as listed in Table III. For different electric fields, J_0 (A/cm^2) has the minimum value at 40% OMR.

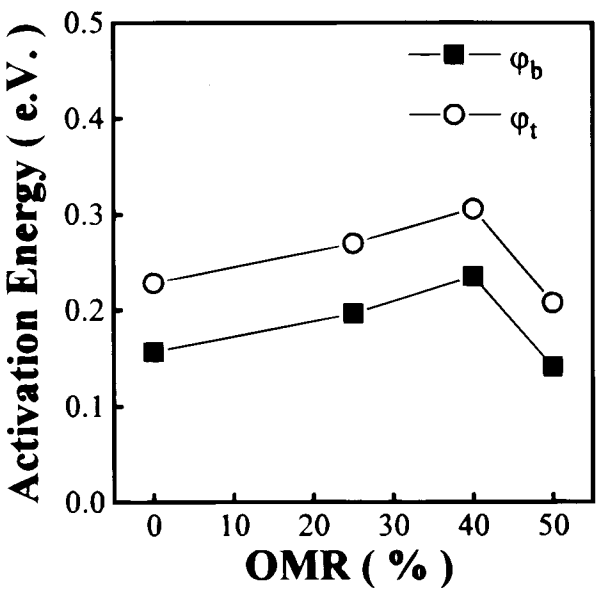

Fig. 13. The variation of activation energy with OMR for BST films.

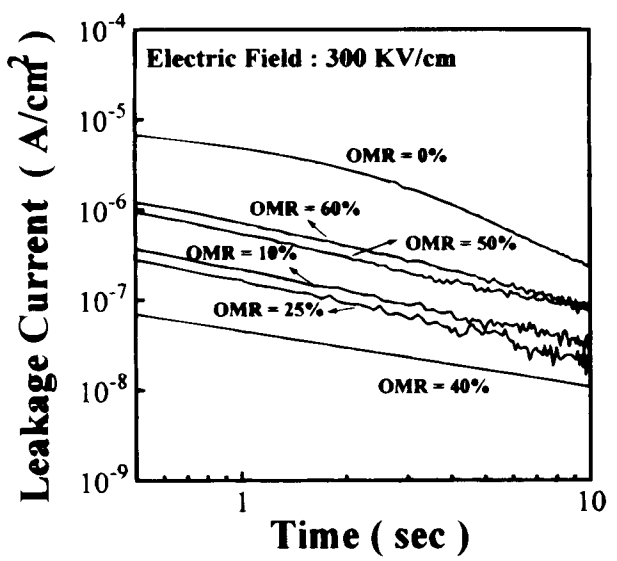

Fig. 14. The positive current-time characteristics of the BST films deposited at various OMR indicated.

Figure 15 shows the variation of leakage current of 50% OMR BST films with time under different dc stress fields. The leakage currents under 1.5, 2.0, and 2.5 MV/cm dc stress fields slowly decrease with stress time, which those under 3.0 and 3.3 MV/cm slowly decrease with stress time in the beginning stage of the stress, and then gradually increase up to the breakdown. For a field less than 2.5 MV/cm, only the slow decrease of current without any following current degradation was observed within the measured time range. The above responses are substantially the same as those reported by Waser for $SrTiO_3$ thin films with a thickness of 200 nm.[26]

Figure 16 shows the *I-V* properties with delay time 30 s for 50% OMR films after stressing at various positive dc fields for 500 s. The *I-V* characteristics after 1.5, 2.0, and 2.5 MV/cm for 500 s have no degradation, but degradation already occurs in the films after stressing at 3.0 and 3.3 MV/cm.

Conclusions

The BST thin films were grown on Pt/SiO_2/Si substrates by rf magnetron sputtering with various OMR ranging from 0 to 60% to change the concentration of oxygen vacancies on the as-deposited films. The current-voltage behavior of the films was analyzed in terms of SE and PF mechanisms. The SE conduction and PF transport mechanisms are observed below and above the transition electric field of 490 kV/cm, respectively, in the BST films prepared at low OMR (0% ~ 25%); and while SE mechanism dominates both below and above 490 kV/cm in the films deposited at high OMR (40 ~ 60%). These results show that concentration variation of the oxygen vacancies induced by the film deposition at various OMR significantly affects the conduction mechanism in the films. The static dielectric constant calculated from *C-V* data are in reasonably good agreement with dynamic dielectric constant obtained from *I-V* data. Therefore, we suggest that the static dielectric constant should be used to describe the carrier transport in 0% OMR BST film. The combination of static and optical dielectric constants should be employed to describe the carrier transport in other higher OMR percent films, since the value of the dynamic dielectric constant was between the static dielectric constant and the optical dielectric constant.

Table III. Extracted current parameters from *J-t* characteristics at room temperature of BST thin film capacitors deposited at various OMR.

OMR (%)	dc Electric field 100 kV/cm J_0 (A/cm^2)	100 kV/cm n	150 kV/cm J_0 (A/cm^2)	150 kV/cm n	300 kV/cm J_0 (A/cm^2)	300 kV/cm n
0	1.6×10^{-6}	0.55	2.4×10^{-6}	0.54	4.8×10^{-6}	0.45
25	4.8×10^{-8}	0.86	8.0×10^{-8}	0.84	1.7×10^{-7}	0.78
40	3.3×10^{-8}	0.84	5.6×10^{-8}	0.84	7.2×10^{-8}	0.77
50	1.8×10^{-7}	0.76	2.9×10^{-7}	0.74	5.5×10^{-7}	0.73

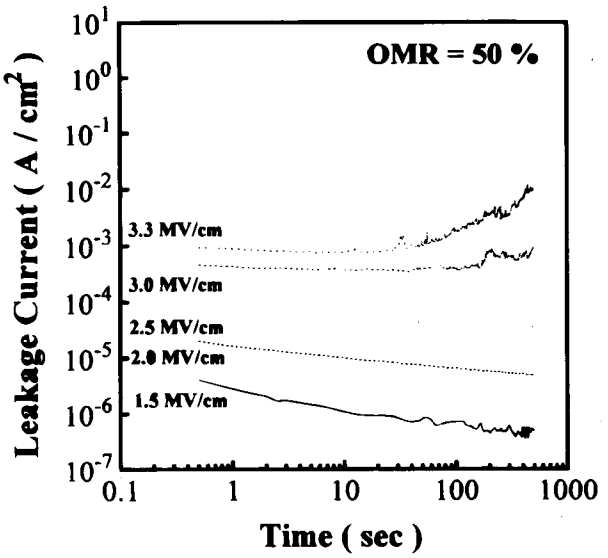

Fig. 15. The leakage current-time properties of 50% OMR BST film under various dc stress fields indicated.

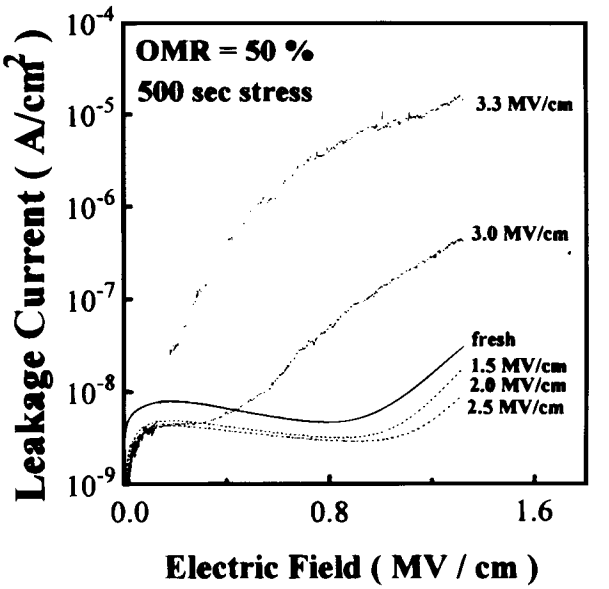

Fig. 16. The *I-V* characteristics with delay time 30 s for 50% OMR BST films after stressing at various fields with 500 s.

Acknowledgments

The authors gratefully appreciate the financial support from the National Science council of R.O.C. under project no. NSC 85-2112-M009-037. Dr. P. Lin is thanked for helpful discussion.

Manuscript submitted October 15, 1997; revised manuscript received February 18, 1998.

National Chiao Tung University assisted in meeting the publication costs of this article.

REFERENCES

1. Y. Ohno, T. Horikawa, H. Shinkawata, K. Kashihara, T. Kuroiwa, T. Okudaira, Y. Hashizume, K. Fukumoto, T. Eimori, T. Shibano, K. Arimoto, H. Itoh, T. Nishimura, and H. Miyoshi, in *1994 Dig. Tech. Papers of the Symposium on VLSI Technol.*, 149 (1994).
2. T. Eimori, Y. Ohno, J. Matsufusa, S. Kishimura, A. Yoshida, H. Sumitani, T. Maruyama, Y. Hayashide, K. Moriizumi, T. Katayama, M. Asakura, T. Horikawa, T. Shibano, H. Itoh, K. Namba, T. Nishimura, S. Satoh, and H. Miyoshi, *Tech. Dig. Int. Electron Devices Meet.*, 631 (1993).
3. E. Fujii, Y. Uemoto, S. Hayashi, T. Nasu, Y. Shimada, A. Matsuda, M. Kibe, M. Azuma, T. Otsuki, G. Kano, M. Scott, L. D. Mcmillan, and C. A. Paz de Araujo, *Tech. Dig. Int. Electron Devices Meet.*, 267 (1992).
4. K. Koyama, T. Sakuma, S. Yamamichi, H. Watanabe, H. Aoki, S. Ohya, Y. Miyasaka, and T. Kikkawa, *Tech. Dig. Int. Electron Devices Meet.*, 823 (1991).
5. T. Y. Tseng, in *Proceedings of the 1996 International Electron Devices and Materials Symposia*, **C2-5**, National Tsing Hua University, pp. 89-96, Hsinchy, Taiwan (1996).
6. T. Mihara and H. Watanabe, *Jpn. J. Appl. Phys.*, **34**, 5664 (1995).
7. T. Mihara and H. Watanabe, *Jpn. J. Appl. Phys.*, **34**, 5674 (1995).
8. P. Li and T. M. Lu, *Phys. Rev. B*, **43**, 14 261 (1991).
9. C. S. Hwang, S. O. Park, H. J. Cho, C. S. Kang, H. K. Kang, S. I. Lee, and M. Y. Lee, *Appl. Phys. Lett.*, **67**, 2819 (1995).
10. C. S. Hwang, S. O. Park, C. S. Kang, H. J. Cho, H. K. Kang, S. T. Ahn, and M.Y. Lee, *Jpn. J. Appl. Phys.*, **34**, 5178 (1995).
11. Y. Shimada, A. Inoue, T. Nasu, K. Arita, Y. Nagano, A. Matsida, Y. Uemoto, E. Fujii, M. Azuma, Y. Oishi, S. I. Hayashi, and T. Otsuki, *Jpn. J. Appl. Phys.*, **35**, 140 (1996).
12. Y. P. Wang and T. Y. Tseng, *J. Appl. Phys.*, **81**, 6762 (1997).
13. M. S. Tsai, S. C. Sun, and T. Y. Tseng, *J. Appl. Phys.*, **82**, 3482 (1997).
14. J. J. Lee, C. L. Thio, and S. B. Desu, *J. Appl. Phys.*, **78**, 5073 (1995).
15. J. H. Joo, J. M. Seon, J. C. Jeon, K. Y. Oh, J. S. Roh, and J. J. Kim, *Appl. Phys. Lett.*, **70**, 3053 (1997).
16. S. T. Kim, H. H. Kim, M. Y. Lee, and W. J. Lee, *Jpn. J. Appl. Phys.*, **36**, 294 (1997).
17. S. M. Sze, *Physics of Semiconductor Devices*, 2nd ed., John Wiley & Sons, New York, 254 (1981).
18. A. M. Cowly and S. M. Sze, *J. Apply. Phys.*, **36**, 3212 (1965).
19. S. M. Sze, *J. Appl. Phys.*, **38**, 2951 (1967).
20. K. C. Kao and W. Hwang, *Electrical Transport in Solids*, 91 (1981).
21. J. H. Simmons, *Phys. Rev.*, **155**, 657 (1967).
22. C. A. Mead, *Phys. Rev.*, **128**, 2088 (1962).
23. S. Banerjee, B. Shen, I. Chen, J. Bohlman, G. Brown, and R. Doering, *J. Appl. Phys.*, **65**, 1140 (1989).
24. J. C. Schug, A. C. Lilly, Jr., and D. A. Lowitz, *Phys. Rev.*, **B1**, 4811 (1970).
25. J. Antula, *J. Appl. Phys.*, **43**, 4663 (1972).
26. R. Waser and M. Klee, in *Proceedings of the 3rd International Symposium on Integrated Ferroelectrics*, p. 288, IEEE (1991).